energies

MDPI

Article

A Two-Stage Sequential Configuration Strategy of PPF and APF for Wind Farm Harmonic Mitigation

Huajia Wang [1], Yan Zhang [1], Wenbin Ci [1], Fan Xiao [2] and Jiawei Luo [2,*]

[1] State Grid Shandong Electric Power Research Institute, Jinan 250001, China
[2] College of Electrical and Information Engineering, Hunan University, Changsha 410082, China
* Correspondence: hhyljw011226@163.com

Abstract

Large-scale wind integration introduces significant harmonic degradation and resonance risks. Traditional strategies primarily targeting Total Harmonic Distortion (THD) often struggle with individual node violations and high investment costs. To address these challenges, this paper proposes a two-stage sequential coordination strategy for Passive Power Filters (PPFs) and Active Power Filters (APFs). First, stochastic harmonic emission and frequency-domain power flow models are developed to characterize wind-induced harmonic propagation. Second, a sequential optimization framework is established to minimize Life Cycle Cost (LCC). In the first stage, PPF siting and sizing are optimized for cost-effective, system-wide mitigation of low-order harmonics while ensuring THD compliance. The second stage utilizes targeted APF deployment to precisely suppress residual high-order violations and localized resonance. Chance-constrained programming is incorporated to manage wind power uncertainty, enhancing the scheme's robustness. Simulations on an IEEE 17-bus system demonstrate that the proposed method effectively balances harmonic suppression performance with economic efficiency, providing a robust and cost-effective solution for wind farm power quality management.

Keywords: wind farm; harmonic emission; chance constraint; harmonic mitigation; sequential allocation

1. Introduction

With the advancement of the "Dual Carbon" goals, wind power, as the core mainstay of renewable energy generation, has witnessed a continuous expansion in its installed capacity and has become a crucial component in the development of China's new power system [1,2]. Grid integration of wind turbines is managed via power electronic converters, driving a paradigm shift in wind farm collector systems. These networks, once dominated by traditional power-frequency equipment, have evolved into highly complex, power-electronics-dominated systems. Although this evolution underpins the flexible and efficient integration of wind energy, it also poses formidable new challenges to internal power quality control and the secure, stable operation of wind farms [3–5].

Harmonic currents across a wide spectrum of frequencies are inevitably generated by the high-frequency switching and nonlinear control strategies of wind turbine power electronic converters. During their propagation through the wind farm's radial collector network, these harmonics are prone to amplification, driven by the line impedances and the distributed parameters of the pad-mounted transformers and collector lines. Consequently,

Check for updates

Academic Editor: Adrian Ilinca

Received: 4 April 2026
Revised: 9 May 2026
Accepted: 15 May 2026
Published: 20 May 2026

Copyright: © 2026 by the authors. Licensee MDPI, Basel, Switzerland. This article is an open access article distributed under the terms and conditions of the Creative Commons Attribution (CC BY) license.

this amplification not only leads to severe THD violations at the Point of Common Coupling (PCC) and internal nodes, but also risks interacting with the system impedance to trigger series or parallel resonances. These resonant conditions further aggravate harmonic distortion, accelerate equipment insulation degradation, and pose a direct threat to the safe and stable operation of primary equipment and reactive power compensators within the facility [6–10]. In contrast to traditional centralized generation, wind power output is highly stochastic and fluctuating. Such uncertainty not only modifies harmonic injection levels but also indirectly leads to deviations in the system's equivalent impedance characteristics and the distribution of resonant frequencies, which further complicates the task of harmonic mitigation within wind farms [11,12].

Installing harmonic mitigation equipment is the prevalent method for resolving harmonic problems arising from wind turbine grid connections. Due to their simple topology and low capital cost, PPFs are highly cost-effective for mitigating specific low-order harmonics and have thus seen widespread application across power systems. To mitigate harmonic pollution in radial distribution networks, Reference [13] presented an approach that employs the Particle Swarm Optimization (PSO) algorithm for the planning and optimization of single-tuned filters. Reference [14] focused on the decline in power quality caused by non-fundamental harmonic issues arising from nonlinear and static loads in radial distribution networks, highlighting the necessity of optimally allocating PPFs to improve system power quality. However, PPFs possess fixed parameters, resulting in limited adaptability to changing operating conditions and high-order harmonic perturbations. Furthermore, they risk introducing new resonances into complex systems. Conversely, APFs dynamically regulate compensating harmonic currents based on real-time system operating conditions, providing robust suppression against a broad spectrum of harmonics and stochastic disturbances. Reference [15] presented a hybrid active power filter (HAPF) control strategy incorporating PSO and adaptive fuzzy techniques. This approach allows the system to identify reactive power and harmonics with greater speed and precision, ultimately resulting in a reduced THD. To solve system-wide harmonic suppression challenges, Reference [16] introduced a clustered APF optimal allocation algorithm based on nonlinear load partitioning, successfully realizing the optimal placement, capacity, and output settings for the active filters. Nevertheless, the high capital costs and operating losses of APFs render their widespread deployment in large-scale power systems highly impractical.

To achieve a balance between mitigation effectiveness and economic efficiency, APF capacity optimization, coordinated operation of multiple compensation devices, and probabilistic filter planning accounting for renewable energy uncertainty have gained significant recognition and application in modern distribution networks [17–20]. Although recent literature has made substantial progress in areas such as multi-device coordination, life cycle cost (LCC) considerations, and multi-objective constraints, a critical research gap persists: existing simultaneous configuration paradigms fail to capture the dynamic evolution of system impedance triggered by the integration of mitigation devices, thereby complicating the prevention of secondary resonance risks derived from basic filtering. The integration of large-capacity PPFs for basic low-order harmonic mitigation fundamentally reshapes the inherent resonance frequency distribution of the wind farm network. This impedance reconfiguration can easily trigger shifts in local high-order harmonic resonance points, leading to severe exceedance or amplification of individual harmonic distortion at specific nodes. Traditional simultaneous planning at a single time-section struggles to predict and effectively suppress these derivative risks, which possess a clear chronological physical causality.

To address this research gap, this paper integrates filtering devices with probabilistic planning theory to propose a two-stage sequential configuration strategy of PPF and APF

for wind farm harmonic mitigation. The main contributions of this paper are summarized as follows:

(1) Construction of a sequentially decoupled PPF-APF coordination framework: Breaking through the limitations of traditional simultaneous solving paradigms, this strategy physically decouples the low-cost basic mitigation of low-frequency characteristic harmonics (via PPF) and the targeted suppression of high-frequency derivative resonance risks (via APF) in chronological order. This engineering logic addresses the resonance frequency shift caused by the integration of large-capacity passive filters.

(2) Proposal of a robust optimization strategy balancing economy and extreme risk: Addressing wind power uncertainty, the model integrates deterministic baseline scenarios with extreme probability scenarios. Through chance-constrained programming, it ensures compliance with power quality standards under the worst-case effective scenario at a 95% probability boundary, achieving an optimal trade-off between LCC and system robustness.

2. Harmonic Power Flow Model for Wind Farm Networks

2.1. Wind Farm Harmonic Frequency-Domain Power Flow Model

Wind farm collection systems typically feature a radial topology with high line impedances and substantial disparities in nodal short-circuit capacities, making their harmonic propagation and amplification behaviors distinctly different from those of traditional transmission and distribution grids. To precisely delineate the wind farm's voltage response to harmonic current perturbations across the full harmonic spectrum, this section evaluates the system's frequency-dependent impedance characteristics and formulates a harmonic power flow model. This model serves to elucidate the propagation and response mechanisms of different harmonic components throughout the network.

For the h-th order harmonic, the harmonic nodal voltage equation can be expressed as:

$$\begin{bmatrix} I_{1,h} \\ I_{2,h} \\ \vdots \\ I_{i,h} \end{bmatrix} = \begin{bmatrix} Y_{11}^{h} & Y_{12}^{h} & \cdots & Y_{1i}^{h} \\ Y_{21}^{h} & Y_{22}^{h} & \cdots & Y_{1i}^{h} \\ \vdots & \vdots & \ddots & \vdots \\ Y_{i1}^{h} & Y_{i2}^{h} & \cdots & Y_{ii}^{h} \end{bmatrix} \begin{bmatrix} U_{1,h} \\ U_{2,h} \\ \vdots \\ U_{i,h} \end{bmatrix} \tag{1}$$

where

$I_{i,h}$ denotes the h-th harmonic injection current from the harmonic source at node I;
$U_{i,h}$ represents the h-th harmonic voltage at node i.

2.2. Sequential Mitigation Framework for Wind Farm Harmonics

Traditional single-type harmonic mitigation devices struggle to strike an optimal balance between mitigation effectiveness and economic efficiency for the following reasons:

(1) Fixed Tuning of PPFs: Although PPFs can effectively reduce harmonic distortion at specific frequencies, their fixed tuning characteristics limit their ability to adapt to varying system operating modes and configurations.

(2) Prohibitive Cost of APFs: APFs offer flexible and superior compensation capabilities, deploying them directly across the entire network often leads to prohibitive investment and maintenance costs.

(3) Limitations of Optimization Paradigms: Current objective functions generally follow two paradigms: single-objective optimization focused on THD minimization, or multi-objective optimization that balances economy and performance. However, both approaches possess inherent limitations. The former fails to account for the trade-off between mitigation costs and device utilization. The latter, due to the strong coupling

between objectives and the highly nonlinear nature of the search space, often causes optimization algorithms to become trapped in local optima.

Addressing these challenges, a two-stage sequential PPF-APF mitigation strategy is presented. The first stage leverages the cost-efficiency of PPFs for the foundational suppression of system-wide low-order characteristic harmonics, ensuring that the THD remains compliant with regulatory limits. Subsequently, the second stage identifies nodes where specific harmonic orders exceed allowable thresholds, deploying APFs for the targeted mitigation of high-order harmonics and potential resonance hazards.

2.2.1. Overall Strategy and Implementation Process of Sequential Mitigation

The schematic diagram of the proposed two-stage sequential mitigation strategy is illustrated in Figure 1.

(1) Stage 1: Global Foundational Mitigation via PPFs

The core objective of this stage is to maintain the THD of all nodes across the wind farm network within national standard limits at a 95% confidence level, while minimizing the overall mitigation cost. Targeting the low-order characteristic harmonics that account for the highest amplitude proportions, this stage optimizes the siting and sizing of PPFs. This achieves low-cost, wide-area foundational harmonic mitigation, establishing a low-harmonic background environment for the refined mitigation in Stage 2.

(2) Stage 2: Precise Reinforcement Mitigation via APFs

Within the unified optimization framework for LCC minimization, the core objective of the second stage is to suppress harmonic amplification and resonance risks at high-risk nodes, ensuring that the individual Harmonic Ratio of Voltage (HRU) at all nodes across the network satisfy national standard limits. Targeting the identified high-risk nodes, the installation locations and capacities of the APF are optimized to achieve dynamic and precise compensation for high-order harmonics and uncertain harmonic disturbances, thereby reinforcing the mitigation effectiveness achieved in the first stage.

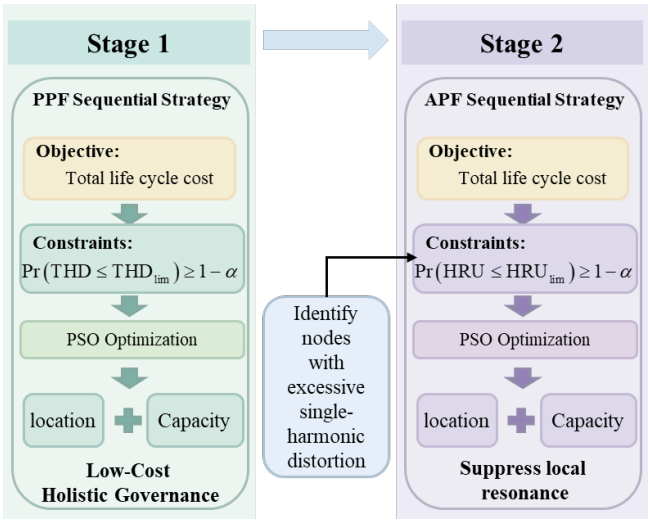


Figure 1. Flowchart of the two-stage sequential governance strategy based on PPF and APF.

2.2.2. Overall Optimization Objective Function

Within the proposed sequential framework, although PPFs and APFs are deployed in distinct phases, they are integrated into a single planning goal—minimizing the total cost while ensuring compliance with power quality standards. Consequently, a unified objective function is utilized for the comprehensive assessment of the dual-stage allocation schemes.

The primary decision variables, along with their physical significance, are summarized as Table 1:

Table 1. Key decision variables and their descriptions.

Variables	Description	Type
Z_i	Whether a mitigation device is installed at node i	Binary variable
$Q_{C,i}$	Passive filter capacity	Continuous variable
$I_{P,i}$	Active filter capacity	Continuous variable

Harmonic mitigation devices are typically capital-intensive assets with extended operational lifespans. Relying solely on initial investment comparisons can easily lead to a "short-term optimal, long-term deficit" decision-making pitfall. Therefore, this paper adopts the internationally recognized LCC theory to uniformly convert investment, operation and maintenance (O&M), and residual value into an Equivalent Annual Cost:

$$\min J = \sum_{i=1}^{N} \left[\left(C_{\text{fix}}^{\text{PPF}} Z_i^{\text{PPF}} + C_{\text{cap}}^{\text{PPF}} Q_{C,i} + C_{\text{fix}}^{\text{APF}} Z_i^{\text{APF}} + C_{\text{cap}}^{\text{APF}} I_{P,i} \right) \cdot CRF + C_{\text{O\&M}}^{\text{PPF}} Z_i^{\text{PPF}} + C_{\text{O\&M}}^{\text{APF}} Z_i^{\text{APF}} \right] \quad (2)$$

$$CRF = \frac{r(1+r)^Y}{(1+r)^Y - 1} \quad (3)$$

where

$C_{\text{fix}}^{\text{PPF}}$ and $C_{\text{fix}}^{\text{APF}}$ signify the fixed expenditures (civil works, commissioning, and grid connection) for PPFs and APFs;

$C_{\text{cap}}^{\text{PPF}}$ is the unit capacity cost of the reactive power compensation capacitor banks;

$C_{\text{cap}}^{\text{APF}}$ is the unit capacity cost of the APF power modules;

CRF is the capital recovery factor, where r denotes the discount rate and Y represents the equipment lifespan;

$C_{\text{O\&M}}^{\text{PPF}}$ and $C_{\text{O\&M}}^{\text{APF}}$ are the average annual O&M costs for PPFs and APFs, respectively, encompassing inspections, spare parts, and insurance.

The cost and life-cycle coefficients for the mitigation equipment are presented in Table 2.

Table 2. Cost coefficients and lifecycle parameters of the mitigation devices.

Parameter	APF	PPF
Fixed cost (10^4 CNY/set)	15	5
Unit capacity cost	0.029 (10^4 CNY/A)	1.5 (10^4 CNY/MVar)
Annual maintenance cost (10^4 CNY/set)	2	0.5
Discount rate (%)	8	8
Lifespan (years)	15	15

The aforementioned overall objective function is consistently applied throughout the entire two-stage optimization process. Both the PPF optimization in Stage I and the APF optimization in Stage II are centered on this objective, ensuring that the resulting mitigation scheme achieves global optimality.

2.3. Stage 1: Optimization Model for System-Wide Foundational Mitigation via PPFs

2.3.1. Principles of Harmonic Mitigation and Frequency-Domain Modeling for PPFs

By creating a low-impedance shunt path at targeted harmonic frequencies, PPFs effectively divert and suppress corresponding harmonic currents. Single-tuned filters, a standard industrial solution, are utilized here to address the dominant low-order harmonics inherent in wind farm networks. As the focal decision variables in Stage I, the PPFs

are optimized for placement and capacity. Specifically, this framework evaluates the deployment of PPFs within a restricted set of candidate nodes proximate to the harmonic sources to enhance mitigation performance.

Upon the integration of a PPF at node i, the h-th harmonic nodal admittance matrix of the system is updated as follows:

$$Y_{h,i} = Y_{h,i}^{0} + Y_{h,i}^{ctrl} \tag{4}$$

$$Y_{h,i}^{\mathrm{ctrl}} = \frac{1}{R + j(h\omega_1 L - \frac{1}{h\omega_1 C})} \tag{5}$$

where

R is the equivalent resistance of the PPF;

ω_1 is the fundamental angular frequency;

L is the PPF inductance value;

C represents the PPF capacitance value;

$Y_{h,i}^{0}$ is the original system admittance for the h-th harmonic at node i and $Y_{h,i}^{ctrl}$ represents the additional admittance term introduced by the mitigation device.

Utilizing the updated admittance matrix, harmonic power flow calculations are performed to derive the individual harmonic voltage magnitudes across the network. To assess the effectiveness of the foundational mitigation in Stage I, the THD is computed for every node. For node i, the voltage Total Harmonic Distortion is defined as follows:

$$\mathrm{THD}_i = \sqrt{\sum_{h=2}^{H} \left(\frac{U_i(h)}{U_i(1)} \right)^2} \tag{6}$$

$$U_i = Z_f \cdot I_s(h) \cdot \frac{Z_f}{Z_{ii} + Z_f} \tag{7}$$

where

$U_i(h)$ and $U_i(1)$ signify the h-th harmonic and fundamental voltage magnitudes at node i;

I_s refers to the background harmonic current injection at the node;

Z_f denotes the equivalent impedance of the passive power filter.

2.3.2. Constraint Conditions for Stage 1 Optimization

In the Stage 1 PPF configuration, the overall goal of harmonic mitigation is to regulate voltage distortion levels within the permissible limits for both planning and operation. Following standard power quality assessment practices, this study adopts THD as the evaluation metric for system harmonics and incorporates it as the primary constraint in the Stage I optimization model.

(1) THD Compliance via Chance Constraints

To address the stochastic fluctuations in harmonic distortion driven by wind power uncertainty, this model employs a chance-constrained formulation. This ensures that the THD at all network nodes remains within regulatory limits across the vast majority of operating scenarios. By quantifying uncertainty risks within a probabilistic framework, chance constraints avoid the potential failures of traditional deterministic methods in extreme cases while effectively balancing conservatism and economic efficiency. The mathematical expression is as follows:

$$\Pr(\mathrm{THD}_i \leq \mathrm{THD}_{i,\mathrm{lim}}) \geq 1 - \alpha \tag{8}$$

where

Pr( ) denotes the probability function;

THD_i is the THD value at node i;

THD_{lim} represents the regulatory limit for harmonic voltage distortion; α is the confidence level. In this study, α is set such that the violation risk is capped at 5%, requiring the system-wide THD to meet the standard in over 95% of the operating scenarios.

The chance constraint is solved using a scenario-based approach. Specifically, typical wind power output scenarios are generated based on the Weibull distribution of wind speeds. Latin Hypercube Sampling (LHS) is then employed to produce S initial scenarios. To optimize the robustness of the mitigation scheme, the model ensures that the THD constraint is satisfied in at least $(1 - \alpha)$S scenarios. This is achieved by analyzing the statistical distribution of THD_i across all scenarios and requiring that $THD_i \leq THD_{lim}$ holds true for a minimum of $(1 - \alpha)$S instances.

(2) PPF Installation Capacity Constraints

To align with the physical limitations of the filtering equipment and prevent overcompensation, the capacity of each PPF unit is constrained within predefined boundaries:

$$0 \leq Q_i^{PPF} \leq Q_{i,max}^{PPF} \tag{9}$$

where

$Q_{i,max}^{PPF}$ is the maximum capacity of a single PPF unit.

2.4. Stage 2: Precise Reinforcement Optimization Model via APFs

2.4.1. Harmonic Suppression Mechanism of APFs

In the harmonic frequency domain, the APF is equivalent to a controlled harmonic current source. By injecting a compensation current that is equal in magnitude and opposite in phase to the harmonic source current, it achieves real-time cancelation of harmonic currents and suppresses harmonic voltage distortion. The compensation current injected at node j for the h-th harmonic is denoted as I_j^{APF} Following the commissioning of the APF, the h-th harmonic voltage at node j can be expressed as:

$$U_j(h) = \sum_{j=1}^{N} Y_{h,j}^{-1} \cdot (I_j^{bg}(h) - I_j^{APF}(h)) \tag{10}$$

where

$Y_{h,j}^{-1}$ is the inverse of the nodal admittance matrix after the integration of PPFs;

I_j^{bg} represents the background harmonic current injection at node j;

I_j^{APF} is the column vector of the harmonic compensation current injected by the APF into node j, which contains non-zero entries only at the APF installation node j and zeros for all other nodes.

2.4.2. Constraint Conditions for Stage 2 Optimization

The primary constraint of this stage is the HRU compliance requirement, which must be satisfied alongside the physical operational constraints of the APF equipment:

(1) HRU compliance requirement

$$\Pr(HRU_i \leq HRU_{lim}) \geq 1 - \alpha \tag{11}$$

where

HRU_{lim} is the permissible limit for the individual harmonic voltage ratio.

Compared to THD, this constraint directly targets individual harmonic frequencies, enabling the precise suppression of high-order harmonic amplification and localized resonance risks. It serves as the core technical basis for the refined mitigation strategy of the APF.

(2) APF Rated Capacity Constraints

To ensure the practical implementability of the optimization results in real-world systems, the compensation capacity of the APF must be constrained within its permissible design limits:

$$0 \le I_j^{\mathrm{APF}}(h) \le I_{j,\max}^{\mathrm{APF}}(h) \tag{12}$$

where

$I_{j,\max}^{\mathrm{APF}}$ is the maximum capacity of a single APF unit.

2.5. System Operational Constraints

To ensure the safety of system operation and the feasibility of selecting the location and sizing of the harmonic mitigation device, the model must satisfy the following constraints:

(1) Fundamental Power Balance and Voltage Deviation Constraints

The fundamental power flow is verified using a deterministic worst-case scenario, specifically by adopting the maximum rated output of wind power resources under typical extreme high wind conditions. This ensures that voltage levels remain within permissible limits even when wind power generation reaches full capacity and reactive power demand is at its peak.

Fundamental power balance equation:

$$\begin{cases} P_{G,i} - P_{L,i} + P_{\mathrm{WT},i}^{\mathrm{nom}} = V_i \sum\limits_{j \in N} V_j (G_{ij} \cos\theta_{ij} + B_{ij} \sin\theta_{ij}) \\ Q_{G,i} - Q_{L,i} + Q_{C,i} = V_i \sum\limits_{j \in N} V_j (G_{ij} \sin\theta_{ij} - B_{ij} \cos\theta_{ij}) \end{cases} \tag{13}$$

where

P_i and Q_i represent the fundamental active and reactive power injections at node i, respectively;

$P_{\mathrm{WT},i}^{\mathrm{nom}}$ denotes the nominal rated power output of the wind resource at node i.

(2) Physical Constraints of Mitigation Devices

This section supplements the constraints on the total number of harmonic mitigation devices to be installed:

$$\sum_{i=1}^{N} z_{i,\mathrm{PPF}} \le N_{\mathrm{PPF,max}} \tag{14}$$

$$\sum_{i=1}^{N} z_{i,\mathrm{APF}} \le N_{\mathrm{APF,max}} \tag{15}$$

where

$N_{\mathrm{PPF,max}}$ and $N_{\mathrm{APF,max}}$ represent the maximum number of PPF and APF arrays, respectively, that may be installed within a wind farm.

3. Case Study System and Simulation Validation Framework

3.1. Refinement of Wind Turbine Harmonic Emission Characteristics

Statistical analysis in Reference [21] further corroborates that both the THD and individual harmonic components exhibit marginal sensitivity to variations in power output, with their probability distributions remaining largely consistent across different power

levels. Consequently, for the purposes of harmonic analysis and mitigation optimization in wind farms, wind turbine generators can be equivalently modeled as multi-frequency harmonic current sources connected in parallel at the integration nodes.

In this model, the fundamental current magnitude is adjusted according to the unit's active power output, while the magnitudes and phase angles of each harmonic order are treated as stochastic variables that follow empirical statistical patterns derived from field measurements. The core of this modeling framework is structured into two primary components: magnitude statistical modeling and phase angle statistical modeling.

3.1.1. Statistical Modeling of Harmonic Amplitudes in Wind Turbines

Field measurements in Reference [22] demonstrate that the magnitude of the h-th harmonic current from wind turbines follows a two-parameter Weibull distribution. Its probability density function (PDF) is expressed as:

$$f(I_h) = \frac{k}{c}\left(\frac{I_h}{c}\right)^{k-1} \exp\left\{-\left(\frac{I_h}{c}\right)^{k}\right\} \tag{16}$$

where

k is the shape parameter of the Weibull distribution;

c is the scale parameter of the Weibull distribution.

Engineering simplifications and equivalent modeling are applied to the distribution patterns according to the specific harmonic frequency:

(1) Low-order harmonics: These harmonics are characterized by large magnitudes and high stability. They primarily originate from the fundamental frequency modulation of the Rotor-Side Converter in Doubly Fed Induction Generators and represent the predominant source of THD violations within wind farms. At these lower orders, the Weibull distribution demonstrates high alignment with the Normal distribution; therefore, an equivalent Normal distribution is adopted. Its probability density function is expressed as:

$$f(I_h) = \frac{1}{\sqrt{2\pi}\sigma_h} \exp\left\{-\frac{(I_h - \mu_h)^2}{2\sigma_h^2}\right\} \tag{17}$$

where

μ_h represents the mean value of the h-th harmonic current magnitude;

σ_h denotes the corresponding standard deviation.

(2) High-order harmonics: While their magnitudes are relatively small, these harmonics exhibit strong stochasticity driven by fluctuations in wind power output. They are highly susceptible to interacting with system impedance, which can trigger harmonic amplification and localized resonance. In this frequency range, the Weibull distribution degenerates into a Rayleigh distribution, which is adopted for equivalent modeling. Its probability density function is expressed as:

$$f(I_h) = \frac{I_h}{b_h^2} \exp\left\{-\frac{I_h^2}{2b_n^2}\right\}, I_h \geq 0 \tag{18}$$

where

b_h is the Rayleigh distribution scale parameter for the amplitude of the h-th harmonic current.

The distribution parameters, such as μ_h, σ_h, and b_h, remain invariant across the entire operational range of the turbine units. While the fundamental current magnitude is scaled

in accordance with the specific operating conditions, the statistical characteristics of the harmonic currents are independent of variations in power output.

3.1.2. Statistical Modeling of Harmonic Phase Angles in Wind Turbines

The harmonic phase angle is a critical determinant in the analysis of multi-machine harmonic superposition within wind farms. Based on the hierarchical stochastic characteristics of phase angles, frequency-dependent statistical models are constructed as follows:

(1) Low-order harmonics: The phase angles of low-order harmonics are synchronized with the fundamental grid voltage and exhibit minimal fluctuations. Consequently, a narrow-band normal distribution is employed for modeling. Its probability density function is expressed as:

$$f(\theta_h) = \frac{1}{\sqrt{2\pi}\sigma_{\theta,h}} \exp\left\{-\frac{(\theta_h - \mu_{\theta,h})^2}{2\sigma_{\theta,h}^2}\right\} \tag{19}$$

where

$\mu_{\theta,h}$ and $\sigma_{\theta,h}$ represent the mean value and the standard deviation of the h-th harmonic phase angle, respectively.

(2) High-frequency harmonics: The phase angles of high-frequency harmonics lack a fixed synchronization relationship and exhibit purely random fluctuations. Accordingly, they are modeled using a continuous uniform distribution within the interval [0, 2π). The probability density function is expressed as:

$$f(\theta_h) = \begin{cases} \frac{1}{2\pi}, & 0 \le \theta_h < 2\pi \\ 0, & \text{Other} \end{cases} \tag{20}$$

Based on the aforementioned magnitude and phase angle models, the phasor expression for the h-th harmonic current of a single wind turbine unit is given by:

$$\dot{I}_h = I_h \cdot e^{j\theta_h} \tag{21}$$

Based on the universal harmonic emission characteristics of wind turbine units, a comprehensive harmonic current source model for a single unit has been developed. By elucidating the magnitude and phase angle distribution patterns across distinct harmonic frequencies, this framework provides a robust modeling foundation for evaluating grid-integrated harmonic impacts and conducting probabilistic analyses of power quality violations in wind farms.

3.2. System Overview

To comprehensively validate the applicability of the proposed PPF-APF two-stage synergistic harmonic mitigation method, a wind farm topology is constructed based on the IEEE 17-node system. Through a comparative analysis between the proposed framework and the traditional APF-only approach, the advantages of the two-stage strategy in harmonic suppression are systematically demonstrated.

The wind farm integrates a total of six wind turbine units, each with a rated capacity of 1.5 MW, bringing the total installed capacity to 9 MW. These units are connected to Nodes 5, 7, 9, 11, 15 and 17 of the collector system. The detailed topology of the case study system is illustrated in the following Figure 2.

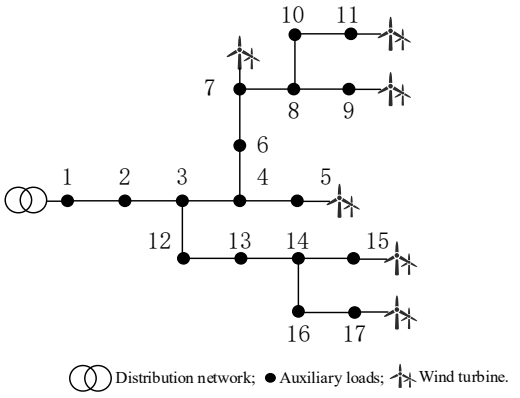


Figure 2. Single-line diagram of the 17-bus wind farm collection grid.

3.3. Wind Power Uncertainty: Scenario Generation and Reduction

This study employs a scenario-based approach to account for the uncertainty of wind power output, providing the necessary scenario support for chance-constrained optimization.

Initially, a two-parameter Weibull distribution is employed to construct the wind speed probability model, characterizing the random fluctuation features of wind power output. Subsequently, the LHS method is utilized to generate 1000 initial wind speed scenarios, which are then mapped to derive the corresponding scenario sets of wind turbine output and harmonic injection. To balance computational accuracy and efficiency, the simultaneous backward reduction method is further applied to reduce the initial scenarios, ultimately extracting 20 typical scenarios. As evidenced by the scatter distribution comparison in Figure 3, the 20 reduced representative scenarios effectively cover the high-probability-density regions of the original 1000 scenarios in a multi-dimensional space, while preserving the boundary scenarios that represent the extreme values of wind power uncertainty. For the model constructed in this paper, once the set of typical scenarios achieves sufficient statistical representativeness, further increasing the number of scenarios provides minimal marginal improvements to the accuracy of the optimization decision, yet it triggers a rapid surge in computational dimensionality. Therefore, retaining 20 scenarios is a rational setting that achieves optimal computational efficiency while ensuring the accurate representation of wind power stochasticity.

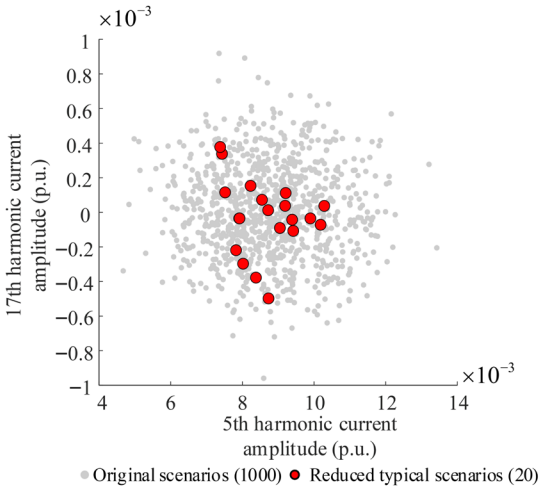


Figure 3. Scatter plot of the original and reduced typical scenarios for the 5th and 17th harmonic currents.

3.4. Design of a Comparative Validation Protocol

To comprehensively quantify and verify the overall advantages of the proposed method, two comparative schemes are designed. To ensure fairness and scientific rigor, the grid constraints, cost parameters, and wind power output simulation scenarios are strictly identical across all schemes; the only difference lies in the configuration strategy of the mitigation devices.

Scheme 1: Traditional full-network APF optimization scheme. This scheme synchronously optimizes the installation locations and capacities of APFs across all nodes in the network. The optimization objective is to minimize the LCC, subject to the constraints that the network-wide THD and individual HRU satisfy national standard limits. Representing the current high-standard single-device mitigation approach, this scheme serves as the comparative baseline for economic and computational efficiency.

Scheme 2: Simultaneous PPF-APF optimization configuration. In this scheme, the installation locations and capacities of both the PPF and APF are optimized concurrently across all nodes within the network. The optimization objective and constraint conditions are identical to those in Scheme 1. This scheme represents the conventional collaborative mitigation approach utilizing multiple types of mitigation devices.

Scheme 3: The proposed two-stage sequential collaborative PPF-APF optimization scheme. This scheme is executed strictly in accordance with the procedure defined in Section 2.2 of this paper: Stage 1 prioritizes the optimal configuration of the PPF to achieve fundamental global mitigation, while Stage 2 conducts a precise supplementary configuration of the APF specifically targeting residual high-order harmonics and the risks of resonance shift. The shared overall objective of both stages is the minimization of the system's total LCC.

4. Results

Based on the aforementioned test system and optimization schemes, a simulation model is established using the MATLAB2024a platform, and the PSO algorithm is employed to solve the optimization problems for all schemes. To ensure the convergence and stability of the algorithm, the key parameters of the PSO are set as follows: the population size is 50, the maximum number of iterations is 200, the learning factors are $c_1 = c_2 = 2$, and the inertia weight ω adopts a linearly decreasing strategy from 0.9 to 0.4 [23].

The mitigation effectiveness of the proposed method is presented in stages, followed by a comprehensive comparative analysis with other comparative schemes from two dimensions: harmonic suppression performance and economic efficiency. The simulation results presented in this paper correspond to the critical effective scenario at the 95% percentile in the uncertainty evaluation. Among the 20 selected typical operational scenarios, this specific scenario lies on the constraint boundary of the probability distribution, with the 19 preceding scenarios fully complying with the standards. The limit violations in the remaining 5% of extreme scenarios fall within the acceptable risk margin permitted by the chance-constrained model when balancing economic efficiency and system reliability.

4.1. Stage 1: Results of Global Foundational Mitigation via PPF

Based on the two-stage optimization framework proposed in this paper, the first-stage optimization for the siting and sizing of PPFs is first conducted. The resulting installation locations, tuning frequencies, and rated capacities of the PPFs are illustrated in Figure 4.

In terms of foundational mitigation performance, the optimized configuration of PPFs has significantly suppressed the low-order characteristic harmonics across all nodes in the wind farm. The statistical THD results for all grid nodes before and after mitigation are illustrated in Figure 5. Following the optimization, the peak THD across the network

dropped from 8.27% to 3.9%, with the average THD stabilized below 3.5%. In 95% of the operational scenarios, the THD at all nodes satisfies the national standard limit of $\leq$4%, successfully fulfilling the Stage 1 objective of "achieving global THD compliance at a low cost."

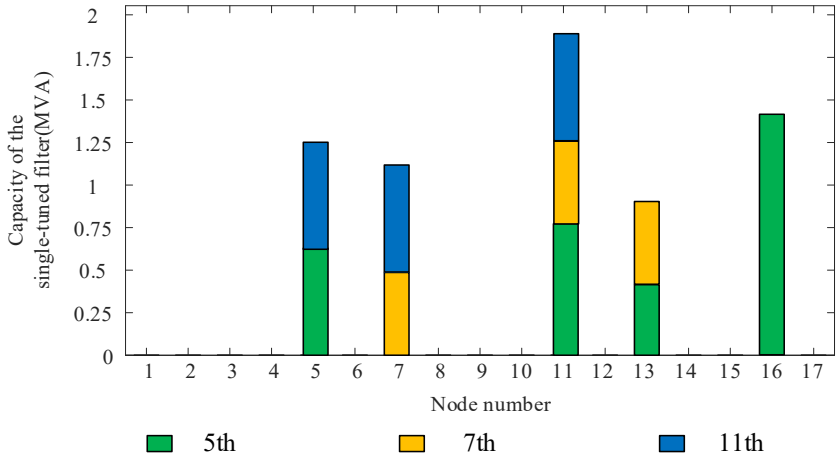


Figure 4. Optimal capacity allocation of single-tuned filters at different nodes.

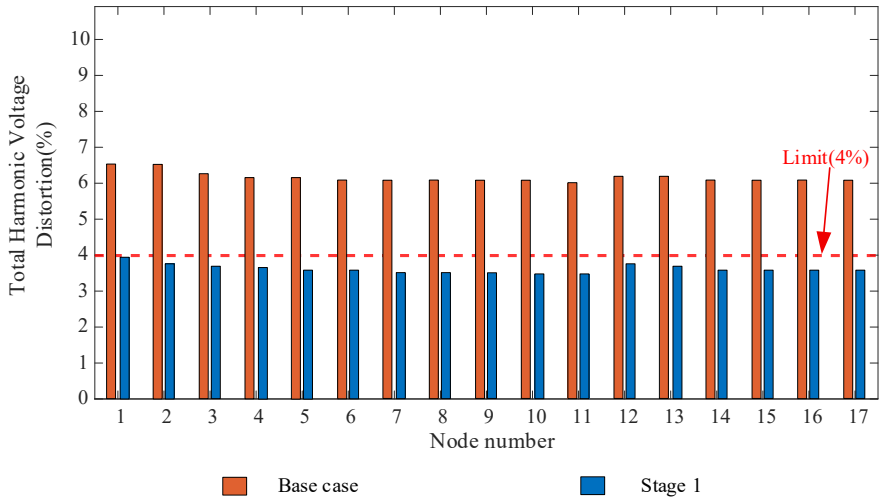


Figure 5. Comparison of total THD at each node before and after Stage 1 mitigation.

Following the Stage 1 mitigation, nodes with individual harmonic content exceeding the limits across the grid-wide full-frequency spectrum are screened to form a set of non-compliant nodes. The 17th harmonic voltage content rates at Nodes 1, 2, and 3 still exhibit violations, with a maximum violation margin reaching 18%. The potential risks of high-order harmonic amplification and localized resonance further confirm the necessity of the Stage 2 precise reinforcement mitigation using APFs.

4.2. Stage 2: Results of Precise Reinforcement Mitigation via APF

Based on the system harmonic distribution characteristics after the first-stage PPF mitigation, nodes where the individual harmonic content rate exceeds the limits across the full frequency spectrum are first screened to form a high-risk node set. Subsequently, strictly adhering to the unified global objective of minimizing the LCC, the installation locations and rated capacities of the APFs are optimized to ensure that the individual HRU of all nodes in the network satisfies national standard limits at a 95% confidence level.

Following the activation of the precisely configured APFs, the high-order harmonic distortions previously identified at the high-risk nodes were effectively suppressed. As

demonstrated by the comparative analysis of individual HRU levels in Figure 6, the targeted compensation provided by the deployment of small-capacity APFs at Nodes 7 and 11 yielded a significant improvement in the system's harmonic profile. The specific compensation capacities of these APF units are detailed in Table 3.

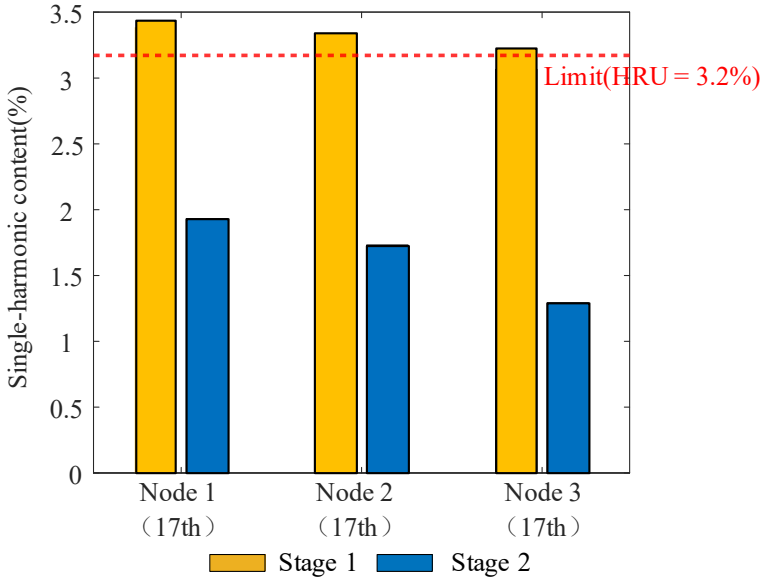


Figure 6. Reduction in the 17th single-harmonic content by the Stage 2 governance strategy.

Table 3. Optimal capacity configuration of the active power filters in Stage 2.

Installation Node	Actual Capacity (A)	Rated Capacity (A)
7	89.8	100
11	84.0	100

After the integration of the APFs, high-order harmonics at high-risk nodes within the wind farm are effectively suppressed. Based on the wind farm topology, the proposed optimization algorithm ultimately allocates small-capacity APFs at Nodes 7 and 11. The mitigation results indicate that this scheme reduces all previously non-compliant HRUs at Nodes 1, 2, and 3 to within the national standard limits, with the maximum HRU dropping from 3.44% to 1.93%. This not only eliminates the individual harmonic violations at these nodes but also prevents potential resonance risks induced by high-order harmonic amplification. It successfully reinforces the mitigation effectiveness of the first-stage PPFs, achieving the comprehensive harmonic mitigation objective characterized by 'global basic mitigation combined with local precise prevention'. Furthermore, the dynamic compensation capability of the APFs effectively addresses the harmonic uncertainties caused by wind power fluctuations. Under all typical operational scenarios, both the THD and individual HRU at all nodes across the network consistently satisfy the national standard requirements, fully verifying the robustness of the proposed sequential mitigation strategy.

From the perspective of the physical mechanism of harmonic mitigation, Nodes 7 and 11, selected by the algorithm, serve as the direct grid integration points for the wind turbines and act as the primary harmonic sources within the wind farm. Configuring APFs at these specific locations essentially achieves local compensation and source-level suppression of harmonics. This strategy directly absorbs high-order harmonic currents at the injection points, physically blocking the propagation of harmonics deeper into the grid and preventing the excitation of secondary resonances with the PPFs. Consequently, it achieves the optimal improvement in network-wide power quality with the minimum

active compensation capacity, clearly demonstrating the engineering economy and technical rationality of the proposed sequential coordinated mitigation framework.

4.3. Comprehensive Techno-Economic Comparative Analysis of Different Configuration Schemes

To quantitatively validate the harmonic mitigation performance of the proposed method, a comparative analysis of the three schemes is conducted from the dual perspectives of economic efficiency and mitigation efficacy.

Figure 7 presents the THD results across all nodes under the unmitigated base case and the three configuration schemes. Prior to mitigation, the THD at all nodes across the network exceeds the 4% national standard limit, indicating severe harmonic violation issues. Although Scheme 1 effectively suppresses the THD at all nodes to within the 4% limit, it relies entirely on the APF for comprehensive harmonic compensation. Lacking the foundational mitigation support from passive filtering devices, it necessitates a massive total APF configuration capacity, which leads to a disproportionately high LCC. In Scheme 2, the post-mitigation THD profile exhibits significant fluctuations across the nodes. This occurs because the parameters of the PPF and APF are globally optimized simultaneously within a single stage. This concurrent approach fails to effectively decouple the complex impedance interactions between the filtering devices and the distribution network, making the system susceptible to local resonance in specific frequency bands. Furthermore, the simultaneous optimization of multiple variables substantially expands the solution space, frequently causing the optimization algorithm to trap in a local optimum. Consequently, the THD at certain nodes (e.g., nodes 8 and 11) severely approaches the 4% limit, reflecting the scheme's insufficient robustness.

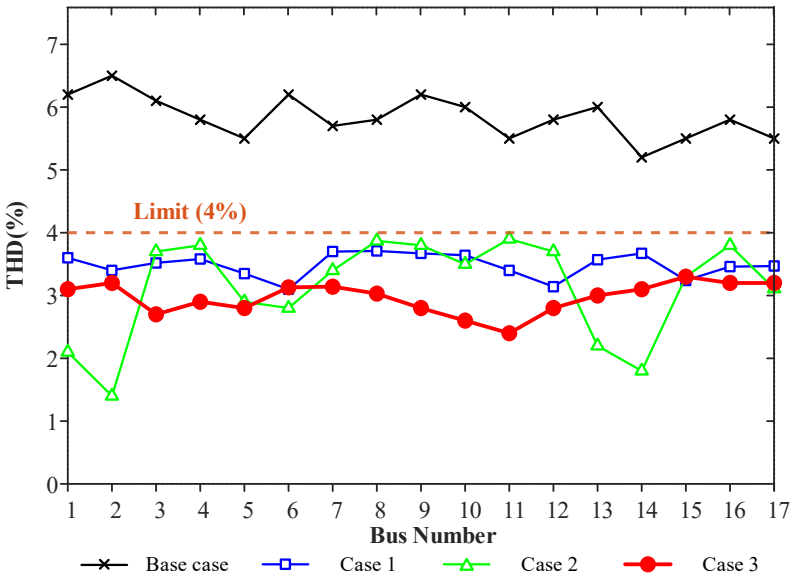


Figure 7. Comparison of THD profiles among different governance cases.

In stark contrast, following mitigation via the two-stage sequential configuration strategy proposed in this paper, the THD profile across the nodes is significantly smoother, demonstrating superior consistency in global harmonic suppression. Through the staged sequential optimization, the proposed strategy not only stably maintains the network-wide node THD at a low level—thereby eliminating the severe THD fluctuations encountered in the simultaneous optimization scheme—but also achieves outstanding economic efficiency while strictly guaranteeing harmonic compliance.

The detailed configuration and operation parameters of each scheme are shown in Table 4.

Table 4. Capacity configuration and economic comparison of different governance cases.

	Phase	Capacity	LCC (104 CNY/Year)	Max THD (%)
Scheme 1	/	231.5 A 198.4 A 251.8 A 213.9 A	18.042	3.71
Scheme 2	/	1.139 MVA, 0.525 MVA 0.775 MVA, 0.723 MVA 1.236 MVA, 1.177 MVA 1.392 MVA, 0.587 MVA 97.8 A, 97.4 A 98.3 A, 110.5 A	26.372	3.92
Scheme 3	Stage 1	1.245 MVA 1.091 MVA 1.882 MVA 0.823 MVA 1.327 MVA	14.632	3.24
	Stage 2	89.8 A 84.0 A		

As demonstrated by the economic comparison results, the LCC of Scheme 3 is merely 14.632×10^4 CNY/year, representing a reduction of 18.90% compared to Scheme 1 and a substantial decrease of 44.52% compared to Scheme 2, thereby highlighting its prominent economic superiority.

These cost discrepancies fundamentally stem from differences in the optimization logic:

Scheme 1 relies exclusively on high-cost active devices for global compensation; the disproportionately large required APF capacity consequently drives up the LCC.

Scheme 2 situates both PPF and APF parameters within a single-stage simultaneous optimization, which drastically escalates the computational complexity. This triggers premature convergence of the algorithm and traps it in a suboptimal local minimum, resulting in severe equipment capacity redundancy. Consequently, the ultimate cost increases rather than decreases. Furthermore, owing to the local optimum induced by simultaneous optimization, the impedance matching between the filtering devices and the system remains poor, failing to avert the risk of local resonance. As a result, its THD strictly approaches the national standard limit, rendering its operational robustness the poorest among the schemes.

In contrast, by decoupling the mitigation objectives through a two-stage sequential optimization, Scheme 3 initially utilizes the low-cost PPF to accomplish the foundational mitigation of low-order harmonics. This substantially curtails the required compensation capacity of the APF. Precise compensation is achieved by configuring minimal APF capacities of only 89.8 A and 84.0 A, thereby eradicating the issue of capacity redundancy at its fundamental source.

5. Conclusions

Addressing the issues of harmonic degradation and resonance risks caused by the grid integration of large-scale wind farms, this paper proposes a PPF-APF two-stage sequential synergistic harmonic mitigation strategy. Simulation results validate the integrated advantages of this method in terms of harmonic suppression, economic efficiency, and robustness.

To enhance the harmonic suppression capability within the wind farm, this study considers a two-stage mitigation strategy: (1) global foundational mitigation optimization via PPF and (2) precise mitigation optimization via APF. By taking the minimization of LCC as the common objective function for both stages, while adhering to their respective constraints, PSO is employed to rationally configure the mitigation devices. This ensures that the goal of minimizing mitigation costs is achieved while strictly satisfying power quality constraints.

The core logic of the proposed sequential coordinated mitigation strategy exhibits structural universality and can be extended to various power quality mitigation scenarios. However, cross-scenario applications require targeted model calibration tailored to the specific characteristics of the target system. Specifically, for distribution networks with a large number of dispersed nonlinear loads, the original radial topology optimization framework must be adapted into a multi-node coordinated model suitable for meshed networks. For ultra-large-scale wind farms integrating long-distance submarine cables, impedance matching analysis must be re-evaluated to address the shifts in system resonance characteristics caused by the distributed capacitance of the cables. Additionally, clustering-based dimensionality reduction algorithms should be employed to mitigate the computational efficiency issues arising from the expanded node scale. Furthermore, parameter drift induced by component aging during long-term equipment operation is a critical variable that must be incorporated to guarantee the life-cycle effectiveness of the mitigation strategy.

Author Contributions: The main idea was proposed by H.W. and Y.Z.; The data and experiment results were collected by H.W., Y.Z. and W.C.; The simulation results were analyzed by H.W., F.X. and J.L.; W.C., F.X. and J.L. wrote the paper. All authors have read and agreed to the published version of the manuscript.

Funding: This research was funded by the Science and Technology Project of State Grid Corporation of China [52062625000C].

Data Availability Statement: The original contributions presented in the study, including the key input parameters and scenario generation settings, are included in the article. Further detailed data and basic simulation scripts that support the findings of this study are available from the corresponding author upon reasonable request.

Acknowledgments: The funding support for our work is greatly appreciated.

Conflicts of Interest: Authors Huajia Wang, Yan Zhang and Wenbin Ci were employed by State Grid Shandong Electric Power Research Institute. The remaining authors declare that the research was conducted in the absence of any commercial or financial relationships that could be construed as a potential conflict of interest. The authors declare that this study received funding from the Science and Technology Project of State Grid Corporation of China [52062625000C]. The funder was not involved in the study design, collection, analysis, interpretation of data, the writing of this article or the decision to submit it for publication.

References

1. Peng, Z.; Xiao, F.; Tu, C.; Wang, L.; Yuan, Y.; Tang, Y.; Guo, X. Optimal Control Strategy for LVRT and Quasi-Synchronous Droop-Controlled Inverter Considering Voltage Drop on the Distribution. *Prot. Control Mod. Power Syst.* **2026**, *11*, 144–158. [CrossRef]
2. Lan, Z.; Tan, R.; Yang, C.; Peng, X.; Zhao, K. Multi-Objective Optimization Method for Flexible Distribution Networks with F-SOP Based on Fuzzy Chance Constraint. *Sustainability* **2025**, *17*, 9510. [CrossRef]
3. Rahman, M.; Dadon, S.H.; He, M.; Giesselmann, M.; Hasan, M. An Overview of Power System Flexibility: High Renewable Energy Penetration Scenarios. *Energies* **2024**, *17*, 6393. [CrossRef]
4. Wang, X.; Chen, X.F.; Ding, L.; Tse, C.K.; Hui, S.Y.R. Constant Output Voltage Three-Phase Capacitive-Power-Transfer Converters With Phase Expansion and Design Methods. *IEEE Trans. Power Electron.* **2026**, *41*, 12331–12343. [CrossRef]

5. Chen, Z.; Wang, X.; Guo, Q.; Tu, C.; Xiao, F.; Li, J. Flexible Reconfiguration Strategy for Novel Advanced Traction Power Supply Equipment Under Fault Conditions. *IEEE Trans. Transp. Electrif.* **2026**. [CrossRef]
6. Sahri, Y.; Tamalouzt, S.; Belaid, S.L.; Bacha, S.; Ullah, N.; Al Ahamdi, A.A.; Alzaed, A.N. Advanced Fuzzy 12 DTC Control of Doubly Fed Induction Generator for Optimal Power Extraction in Wind Turbine System under Random Wind Conditions. *Sustainability* **2021**, *13*, 11593. [CrossRef]
7. Alduraibi, A. Analysis of Harmonics Generated by Power Converters in Power Networks: Impacts and Mitigation Techniques. Ph.D. Thesis, School of Information Technology and Electrical Engineering, The University of Queensland, Brisbane, Australia, 2021. [CrossRef]
8. Wu, D.; Seo, G.-S.; Xu, L.; Su, C.; Kocewiak, L.; Sun, Y.; Qin, Z. Grid Integration of Offshore Wind Power: Standards, Control, Power Quality and Transmission. *IEEE Open J. Power Electron.* **2024**, *5*, 583–604. [CrossRef]
9. Dheyaa, I.M.; Goksu, G. Design and Control of Three-Phase Power System with Wind Power Using Unified Power Quality Conditioner. *Energies* **2022**, *15*, 7074. [CrossRef]
10. Cecati, F.; Becker, J.K.M.; Pugliese, S.; Zuo, Y.; Liserre, M.; Paolone, M. LTP Modeling and Analysis of Frequency Coupling in PLL-Synchronized Converters for Harmonic Power Flow Studies. *IEEE Belgrade Powertech* **2023**, *14*, 2890–2902. [CrossRef]
11. Jie, Y.; Corinna, M.; Tuhfe, G.; Mark, K.; Arne, W.; Gregor, G. Uncovering Wind Power Forecasting Uncertainty Sources and Their Propagation Through the Whole Modelling Chain. *Renew. Sustain. Energy Rev.* **2022**, *165*, 112519. [CrossRef]
12. Muhammad, B.A.; Ahmed, A.; Fei, G. A Coordinated Optimal Operation of a Grid-Connected Wind-Solar Microgrid Incorporating Hybrid Energy Storage Management Systems. *IEEE Trans. Sustain. Energy* **2024**, *15*, 39–51. [CrossRef]
13. Muhira, D.F.; Andi, F.; Christiono; Usman, A.M.; Andi, N.P. Single Tuned Filter Planning to Mitigate Harmonic Polluted in Radial Distribution Network Using Particle Swarm Optimization. In Proceedings of the 2020 3rd International Seminar on Research of Information Technology and Intelligent Systems (ISRITI), Yogyakarta, Indonesia, 10–11 December 2020; pp. 418–422. [CrossRef]
14. Chegudi, R.R.; Balamurugan, R.; RamaKoteswara, R.A. Artificial Rabbits Optimization Based Optimal Allocation of Solar Photovoltaic Systems and Passive Power Filters in Radial Distribution Network for Power Quality Improvement. *Int. J. Intell. Eng. Syst.* **2023**, *16*, 100–109. [CrossRef]
15. Waleed, R.; Khan, A.; Almogren, A.; Arshad, J.; Yousaf, A.; Jaffery, M.H.; Rehman, A.U.; Shafiq, M. Adaptive Fuzzy Logic Controller for Harmonics Mitigation Using Particle Swarm Optimization. *Comput. Mater. Contin.* **2022**, *71*, 4275–4293. [CrossRef]
16. Yang, Z.; Yi, H.; Zhuo, F.; Yin, X.; Wei, W.; Zhang, Y.; Zhang, H.; Wang, Q. Optimal Siting, Sizing and Outputting of Multiple SAPFs under Intelligent Nonlinear Loads Partitioning for System-Level Harmonic Mitigation. *IEEE J. Emerg. Sel. Top. Power Electron.* **2023**, *11*, 2600–2617. [CrossRef]
17. Elkholy, A. Harmonics Assessment and Mathematical Modeling of Power Quality Parameters for Low Voltage Grid Connected Photovoltaic Systems. *Sol. Energy* **2019**, *183*, 315–326. [CrossRef]
18. Lin, L.; Jia, Q.; Lv, C.; Liang, J.; Luo, P. Partitional Collaborative Mitigation Strategy of Distribution Network Harmonics Based on Distributed Model Predictive Control. *IEEE Trans. Smart Grid* **2023**, *14*, 1998–2009. [CrossRef]
19. Kularbphettong, K.; Boonseng, C. HPFs Filtering Solutions for Reduced the Harmonic Current Generated by SMPS and Ac Drive Systems. *Energy Rep.* **2020**, *6*, 648–658. [CrossRef]
20. Zhang, Y.; Klabunde, C.; Wolter, M. Frequency-Coupled Impedance Modeling and Resonance Analysis of DFIG-Based Offshore Wind Farm with HVDC Connection. *IEEE Access* **2020**, *8*, 147880–147894. [CrossRef]
21. Babak, B.; Manoj, G. Practical Experiences and Mitigation Methods of Harmonics in Wind Power Plants. *IEEE Trans. Ind. Appl.* **2013**, *49*, 2279–2289. [CrossRef]
22. Tentzerakis, S.T.; Papathanassiou, S.A. An Investigation of the Harmonic Emissions of Wind Turbines. *IEEE Trans. Energy Convers.* **2007**, *22*, 150–158. [CrossRef]
23. Li, Z.; Xiong, J. Reactive Power Optimization in Distribution Networks of New Power Systems Based on Multi-Objective Particle Swarm Optimization. *Energies* **2024**, *17*, 2316. [CrossRef]

Disclaimer/Publisher's Note: The statements, opinions and data contained in all publications are solely those of the individual author(s) and contributor(s) and not of MDPI and/or the editor(s). MDPI and/or the editor(s) disclaim responsibility for any injury to people or property resulting from any ideas, methods, instructions or products referred to in the content.